Nanoscale Res Lett (2010) 5:180–188
DOI 10.1007/s11671-009-9462-z

NANO EXPRESS

Deposition of Size-Selected Cu Nanoparticles by Inert Gas Condensation

M. Gracia-Pinilla · E. Martínez · G. Silva Vidaurri · E. Pérez-Tijerina

Received: 17 June 2009 / Accepted: 4 October 2009 / Published online: 6 November 2009

Abstract Nanometer size-selected Cu clusters in the size range of 1–5 nm have been produced by a plasma-gas-condensation-type cluster deposition apparatus, which combines a grow-discharge sputtering with an inert gas condensation technique. With this method, by controlling the experimental conditions, it was possible to produce nanoparticles with a strict control in size. The structure and size of Cu nanoparticles were determined by mass spectroscopy and confirmed by atomic force microscopy (AFM) and scanning electron transmission microscopy (STEM) measurements. In order to preserve the structural and morphological properties, the energy of cluster impact was controlled; the energy of acceleration of the nanoparticles was in near values at 0.1 ev/atom for being in soft landing regime. From SEM measurements developed in STEM-HAADF mode, we found that nanoparticles are near sized to those values fixed experimentally also confirmed by AFM observations. The results are relevant, since it demonstrates that proper optimization of operation conditions can lead to desired cluster sizes as well as desired cluster size distributions. It was also demonstrated the efficiency of the method to obtain size-selected Cu clusters films, as a random stacking of nanometer-size crystallites assembly. The deposition of size-selected metal clusters represents a novel method of preparing Cu nanostructures, with high potential in optical and catalytic applications.

Keywords Cu nanoparticles · Inert gas condensation · Cu cluster films · Structure of nanoscale materials

M. Gracia-Pinilla · G. S. Vidaurri · E. Pérez-Tijerina
Facultad de Ciencias Físico-Matemáticas, Universidad Autónoma de Nuevo León, San Nicolás de los Garza, Nuevo León 66450, México
e-mail: miguel.graciapl@uanl.edu.mx

E. Pérez-Tijerina
e-mail: eduardo.pereztj@uanl.edu.mx

M. Gracia-Pinilla · G. S. Vidaurri · E. Pérez-Tijerina
Centro de Innovación, Investigación y Desarrollo en Ingeniería y Tecnología, Laboratorio de Nanociencias y Nanotecnología (CIIDIT-UANL), PIIT Monterrey, Apodaca, NL 66600, México

E. Martínez (✉)
Centro de Investigación en Materiales Avanzados, S.C.(CIMAV), Av. Alianza Norte #202, Parque de Investigación e Innovación Tecnológica (PIIT), Nueva Carretera Aeropuerto Km. 10, Apodaca, Nuevo León 66600, México
e-mail: eduardo.martinez@cimav.edu.mx

Introduction

Owing to their unique catalytic, electronic, magnetic, and optical properties, different from their bulk species, nanoparticles continue to attract the attention of researchers [1]. Metal nanoparticles (NP's) have been synthetically produced by different techniques for many years [2–8]. The approach described in this paper is an inert gas condensation (IGC) technique used before for synthesis of metal NP's [9–12]. The optical, electronic, and thermal properties of metal NP's endow them with potential application in electrical and third-order nonlinear optical devices [13–18], solid dielectric materials [19], nano-biomaterials [20], and high thermal conductivity nanofluids [21]. Recently, attention has been focused on Cu nanoparticles due to their optical and catalytic properties [22–25]. Particularly, the optical and catalytic behavior in Cu nanoparticles is not well understood. It is believed that absorption of light by metal nanoparticles is dominated by the surface plasmon (SP) resonance changing both the static and dynamic optical

properties. These and other properties depend on their size, size distribution, shape, and structure in addition to the interaction between the surfaces of the nanoparticle. Control of these features is not trivial as Cu nanoparticles formation is extremely sensitive to reaction conditions [26, 27]. Although a variety of techniques for the production of Cu nanoparticles have been developed, the main problem is still the control of size that let us to explain the size effects on its properties. In the present work, we describe the synthesis of Cu nanoparticles using a grow-discharge sputtering with an inert gas condensation (IGC) technique. The resulting nanoparticles were analyzed by mass spectroscopy, scanning transmission electron microscopy, and atomic force microscopy. We present the results of the different experimental analysis of the Cu NP's and these results are discussed and contrasted for different experimental conditions.

Experimental

Copper NP's were produced with a sputtering system NanoSys 500, nanoparticles source from Mantis Deposition Ltd. [28]. A schematic of the experimental set-up employed in our laboratory for the production of size-selected Cu clusters is sketched in Fig. 1. In this figure is shown the main parts of the system that consists of a nanocluster source that includes a dc magnetron sputtering unit and the turbomolecular pump (300 l/s), a quadrupolar mass filter, and the deposition chamber where occurs a turbomolecular pumping (1,000 l/s).

The nanocluster source is the heart of the system to obtain the Cu nanoparticles and consists mainly of a device called Nanogen 50, where nanoclusters are generated and then channeled to the main deposition chamber to deposit onto a substrate as shown in Fig. 2. The size-selected Cu nanoparticles deposition takes place through four main processes: Sputtering, aggregation, filtering, and deposition, which we explain in the following to clarify the process.

Cu Clusters Sputtered

The dc magnetron type discharge is used to generate clusters from the target, connected to the magnetron assembly. The magnetron-based source has an advantage over all other types of cluster sources in terms of the wide cluster size range, which varies from fraction of a nanometer to a few tens of nanometers.

DC plasma is ignited in a mixture of argon (Ar) and helium (He) gases and confined close to the Cu target by the magnetic field of the magnetron set-up. In the IGC process, a supersaturated vapor of Cu atoms is originated by sputtering a Cu target in an inert gas atmosphere of Ar and He. The Nanogen system was kept at low temperature by a coolant mixture, and before the nanoparticles deposition, the system pressure was set at 1×10^{-8} Torr. The cluster size can be adjusted by varying three main source parameters: the length over which the clusters aggregate (variable using a linear drive), the power to the magnetron, and the flow of the aggregation gases. In terms of the cluster size range, the magnetron-based source has the advantage over all other types of cluster source as it is the most flexible. For a large number of materials, the source is capable of producing clusters consisting of a few tens of atoms up to particles with diameters of around 20 nm. Due to the nature of the gas aggregation technique, narrow size distributions can be achieved.

Cluster Aggregation

Typically, sputtered clusters are swept through the aggregation region (10^{-1} Torr) by argon and helium gases, where these clusters nucleate to form a distribution of

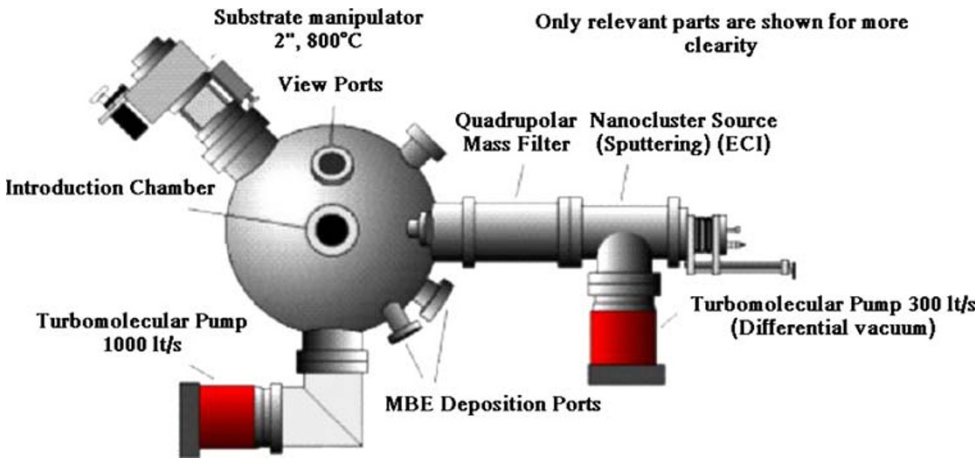

Fig. 1 Integral system to synthesize Cu nanoparticles (image taken from Nanosys500 Manual [28])

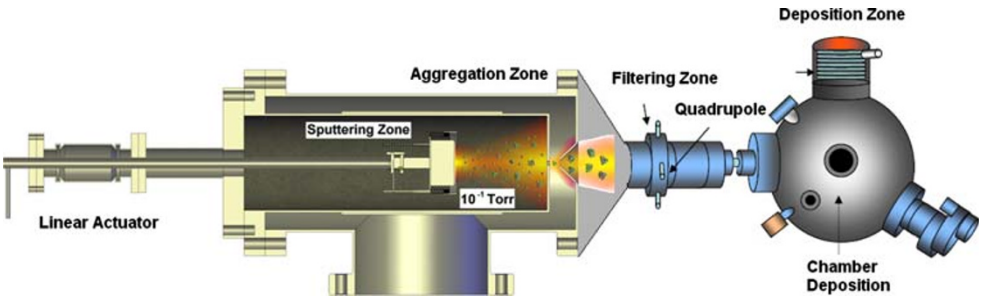

Fig. 2 Schematic diagram of the nanocluster source

nanoclusters of various sizes as represented in Fig. 2. Energetic Cu atoms sputtered from the target are cooled by the He gas leading to the nucleation of clusters. The nucleation of these small cluster 'seeds' is followed by the growth of the seeds into larger clusters. The growth of clusters is heavily dependent of interatomic collisions; this states the importance of Ar and He. Once the Cu clusters grow in size to exceed a critical radius, large clusters grow from the cluster seeds at a faster rate than that at which new seeds are formed. Since He is primarily responsible for the cluster-condensation process, the He partial pressure is used to control the cluster size distribution. The residence time within the aggregation zone can be varied by varying the length of the aggregation region with the linear motion drive. By controlling the aggregation length, and the residence time, one can control the distribution of the nanocluster size within the aggregation region. The nucleation and growth of clusters ceases after expansion through a nozzle where clusters expands into the filtering zone, which is maintained at a much lower pressure (10^{-4} Torr). In our system, the experimental conditions restrict the size of the nanoparticles in the range of 1–20 nm governed by the thermodynamic stabilities related to the cluster binding energies and recombination processes.

Cu Clusters Filtering

Along with the nanocluster source, our system also consists of a quadrupole mass filter (MesoQ), intercepted between the nanocluster source and the main deposition chamber. A large percentage of the Cu clusters generated by the source are ionized, typically 40% for Cu clusters, which makes possible manipulate them electrostatically by the mass filter. MesoQ is used to filter nanoclusters of a particular size from the widely varied size distribution of nanoclusters present in the aggregation region. This mass filter has been specifically added for the purpose of high-resolution measurement and filtering of nanoclusters between 1×10^3 and 3×10^7 a.m.u. The MesoQ utilizes the high ionized content of clusters generated by the Nanogen 50 to achieve a high transmission and to acquire clear mass spectra. The electronics unit allows us to acquire a mass scan of the clusters from the source and filter the ionized clusters.

Clusters Deposition

The focused cluster beam is then mass-selected by a mass spectrometer and then accelerated by a high-voltage pulse applied to a substrate in a high-vacuum chamber with a base pressure of 10^{-8} Torr. The system is capable of depositing at rates between <0.001 nm/s and >0.5 nm/s measured at a distance of 100 mm for Cu clusters. The deposition rate achieved depends on a number of parameters, which includes the material and the size of the clusters deposited. In our case, in the deposition we applied one bias voltage between the substrate (negative) and the chamber, and for this reason we only working with the positive ions. The size of the nanoparticles was controlled through the variation in (1) gas flow (Ar and He), (2) partial pressure, (3) magnetron power, and (4) zone condensation length. These parameters were varied to produce particles of different sizes onto Si substrates. The latter choice was taken for purposes of analysis in a SEM, Nova200 Nanosem. The average size of the nanoparticles was monitored in situ from the synthesis conditions by a linear quadrupole to measure the mass distribution and to act as a mass filter. AFM imaging and manipulation experiments were carried out using a Veeco Instrument Multimode scanning probe microscopy by hard tapping mode (low amplitude setpoint voltage).

Results and Discussion

Nanocluster Size Variation with Experimental Parameters

Ar and He Flow Rate

On changing the operating conditions, the distribution of clusters can be varied and, therefore, the nanocluster source can be calibrated for optimum performance and for selecting the wished cluster size. Figure 3a shows the mass

spectrum of copper nanoparticles deposited on Si substrates under 10, 30, 50, 70, and 90 sccm Ar flow rates where deposition times were fixed for all deposition processes. Nanoparticles of different sizes are clearly visible on the mass spectrums. It is observed that the mean nanoparticle size value of the distribution first increases with an increase in the Ar flow rates to finally decrease for higher Ar flow rates. Physically, the cluster growth phenomenon involves several processes such as embryo formation through three body collision, nucleation by cluster–cluster collision, cluster growth via atomic condensation. Ar flow rate favors the cluster growth because it favors a higher sputter rate besides a better ionization and hence, more rapid cluster formation. However, when a Ar flow rate reach some value the mean cluster size decreases since Ar will also sweep the cluster through the aggregation zone more rapidly, this reducing the time for particle growth. The cluster growth rate strongly depends on the collision probability between clusters, and this collision probability can be increased by increasing the time spent by a cluster within the growth region. So, an increase in the gas flow rate of the carrier gas and, hence, the drift velocity of the material within the growth region decreases the time-of-flight of the clusters, and the collision probability of the clusters also decreases. Additionally, it was observed a clear dependence with He from which a continuous decreasing in mean cluster size is found with the increasing in He flow rate as shown in Fig. 3b. The evident fall in intensity of the cluster beam at higher He flow rate is probably due to the greater efficiency of helium in sweeping the clusters out of the condensation chamber. Higher He flow rates reduces the average particle size by reducing the associated residence time in the aggregation zone due to a higher drift velocity of the Cu clusters within the growth region, similar to which occurs with Ar for high flow rates.

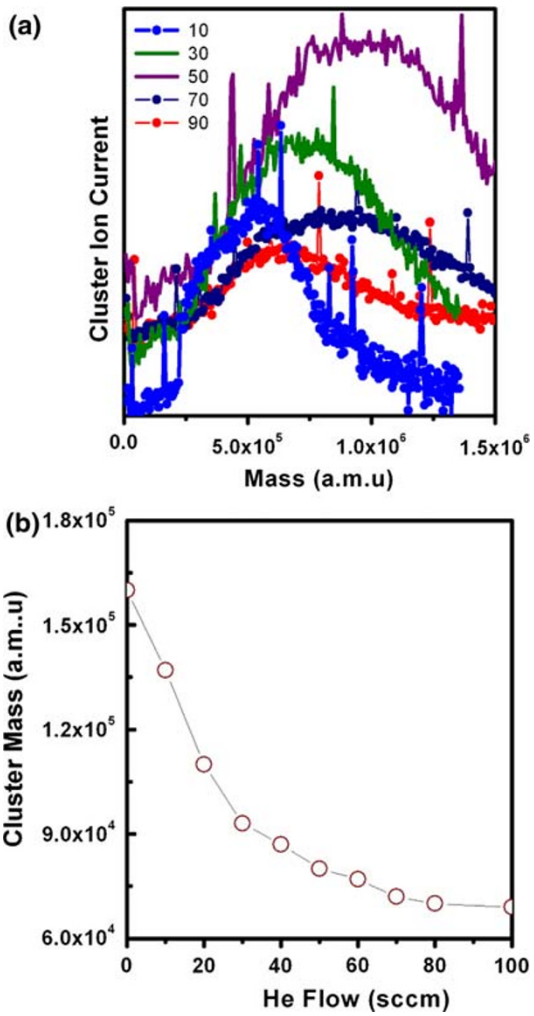

Fig. 3 **a** Cu mass spectra profiles varying the Ar flow rate, **b** Relation between mean cluster mass and He flow rate

Magnetron Power and Aggregation Length

The magnetron power was varied for a fixed aggregation length, Ar and He flow rates, 25 and 2 sccm, respectively. The resulting mass spectra are shown in Fig. 4a from which we observe the strong dependence between mean cluster mass and magnetron power for Cu nanoparticles growth. It can be observed that Cu nanoparticle size has a nearly linear relationship with the sputtering power of the cluster source. The increasing in mean Cu cluster mass with the increasing in magnetron power, it is explained in terms of the higher ionization rate as a consequence of the magnetron power supplied leading to a higher beam intensity. Furthermore, Cu ions count with the aggregation length was varied for fixed experimental parameters (60.3 W, Ar: 25 sccm and He: 2 sccm). The results obtained from mass spectra are shown in Fig. 4b. It is observed that reducing the distance, i.e. aggregation length, from the magnetron head to the first expansion aperture reduces the distance and time whereby condensation can occur so the average nanoparticle size is reduced. We have found that from all the parameters influencing the nanoparticle size, the growth distance is the most determinant. Increasing the growth distance increases the length of time; the clusters have to grow before passing through the nozzle. In the case of Cu nanoparticles, it is possible to move the maximum from around 1 nm to 15 nm by increasing the growth distance from 30 to 130 mm; larger sizes are reached when the other experimental parameters are changed. Copper clusters were detected with the minimum growth distance, which could be explained by the small nucleation barrier ($\Delta G/kT$) for Cu clusters formation. Clusters containing just one nanometer of diameter each were easily produced.

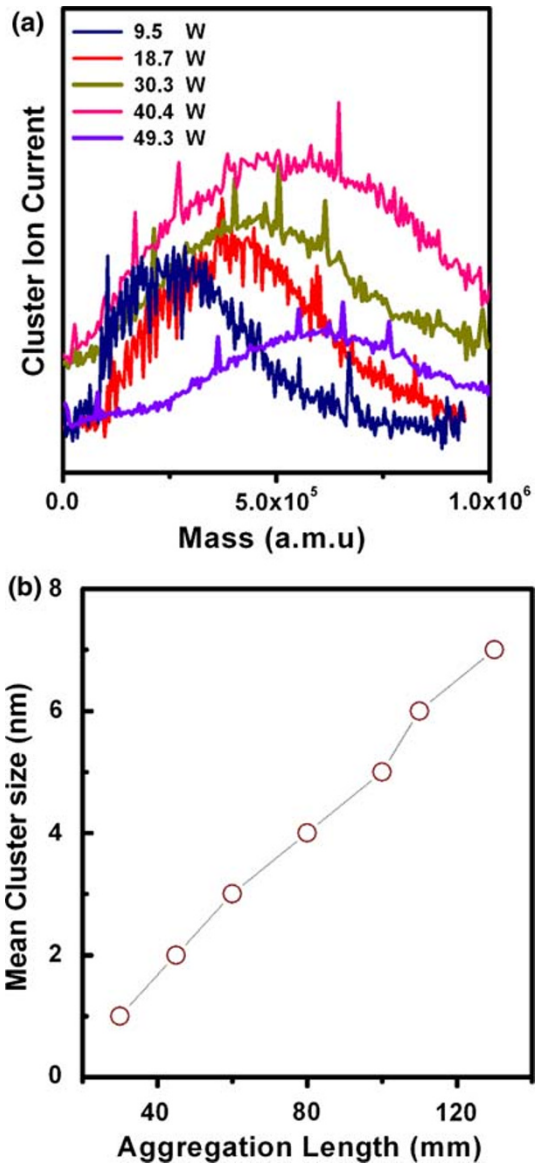

Fig. 4 **a** Cu mass spectra profiles varying the magnetron power and **b** the aggregation length

Monodispersed Cu Nanoclusters: Structural and Morphological Analysis

In order to preserve the structural and morphological properties, the energy of cluster impact was controlled; the energy of acceleration was close to 0.1 eV/atom. High angle annular bright field image (HAADF)-STEM pictures of 5 nm filtered Cu nanoparticles were acquired to obtain the size distribution of the deposited nanoclusters onto carbon coated grids as shown in Fig. 5a. In this figure is possible to distinguish as dotted circles, nanoparticles with 5 nm as they were filtered through the MesoQ. Lower magnification is also presented in Fig. 5b for a better observation of dispersed nanoparticles as well to make size

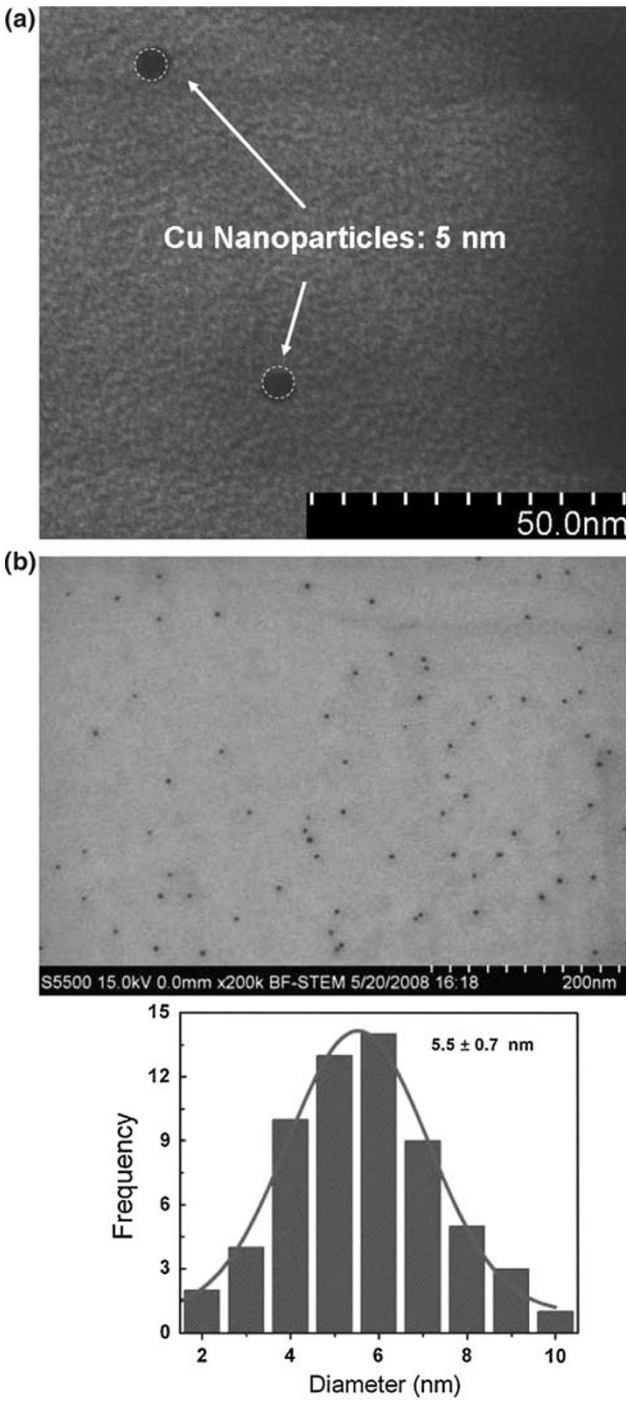

Fig. 5 STEM-HAADF images of soft landed and monodispersed Cu NPS filtered in 5 nm at different magnifications **a** 50 nm **b** 200 nm. Histogram in 5 **b** shows the size distribution

measurements. Histogram in Fig. 5b let us to analyze the mean size by measurements, which demonstrates a narrow dispersion in cluster size filtered at 5 nm with a central value in 5.5 nm, and the effectiveness of technique to obtain nanoparticles of predetermined size. The size distributions indicate the good monodispersivity besides the

fine control of cluster size. Our results showed an excellent agreement between the Cu nanoparticles filtered in 5 nm and those measured by STEM images. Similar results have been reported by other groups [12, 30–33]. A study by HRTEM on these samples is being developed to determine the crystallographic and morphologic features as function of size and will be reported briefly.

The nanoparticle size distribution was also verified using atomic force microscopy in order to obtain the dimensional characteristics of single nanoparticles and statistical data of Cu assembly. AFM observations were developed on the so-called tapping mode that measures the modification of the tip oscillation amplitude due to the tip-sample interactions. Figure 6 shows an AFM image with the corresponding topographical representation in (a) and an amplification of a selected area for a better observation of nanoparticles in (b), where we indicate with a line the path along the height profiles were taken. Height measurement from a selected area is shown in (c). Whereas AFM measurements of distances in the *z*-axis are directly related to the real height of structures, it is well known that distances laying on the *xy*-plane must not be interpreted as the real spatial dimensions since at this dimensional range, the width of the AFM tip is comparable to the diameter of nanoparticles. The width of the objects is distorted due to the combination of the tip and sample geometries, so any measured distance is increased as much as an order of magnitude. Taking this in consideration is not surprising that diameter of nanoparticles looks larger than the real size. For a right analysis, we considered the height (*z*-axis) of nanoparticles as its real size. As obtained by STEM analysis, the size distributions observed in Fig. 6a show the monodispersivity and root mean square roughness of 0.4 nm for nanoparticles filtered in 2 nm. It is worth a mention that height measurement from the selected Cu nanoparticle shown in Fig. 6b was 2.4 nm, which is in excellent accordance with the 2 nm selected Cu clusters fixed experimentally. This fact was present in all nanoparticles measured, which demonstrates the high efficiency of the synthesis method to control the Cu cluster size.

AFM images for nanoparticles deposited on sapphire and filtered in 1 nm reveals similar results as indicated in Fig. 7a. Topographical observation let us distinguish dispersed nanoparticles with a uniform and narrow distribution in size over larger areas on the substrate as indicated in histogram in Fig. 7b obtained through the height profiles measurements as shown in (c). In Fig. 7d, a line indicates the path along the height profile taken by amplification from (a). In this case, the height measurement was 1.05 nm. This fact proves that controlling experimental conditions in soft landing regime let us to control the size cluster with narrow size distribution, which is a critical factor for potential applications, advantage not present in chemical methods.

Cu Cluster Films

Although the main focus in this paper is the understanding of mean Cu cluster size dependence with experimental parameters, it is worth pointing out the appeal of nanostructured Cu films to know the effect of controlling the mean cluster size before deposition on the growth mechanisms and thin film morphology once deposited on a substrate. It is known that the magnetic, optical, and mechanical properties of nanostructured films can be intrinsically different from their macrocrystalline counterparts as has been investigated for nanocrystalline copper or other metal nanoparticles [29, 30]. Our strategy for growing Cu thick films consisted in depositing low energy nanoparticles in which, we try to conserve the memory of the free-cluster phase to form thin films with their original properties in soft-land regime. Cu cluster films were

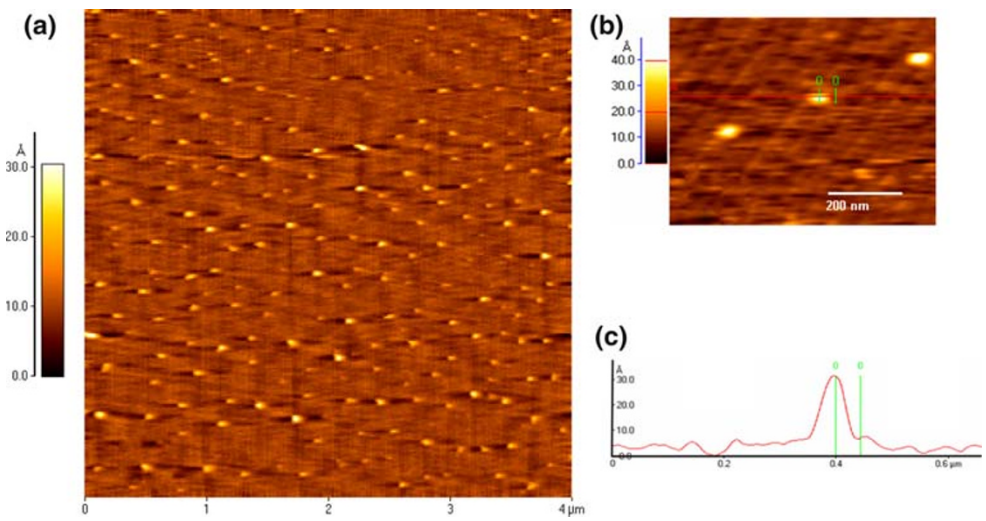

Fig. 6 **a** AFM topographical image from Cu nanoparticles deposited on Si and filtered in 2 nm, **b** Larger magnification of the Cu NPs, **c** *Z*-Height profile along the line indicated in (**b**), height (2.4 nm). Experimental conditions: Ar (20.9 sccm), He (10.9 sccm), Agg. Length (103 mm), Power (60 W)

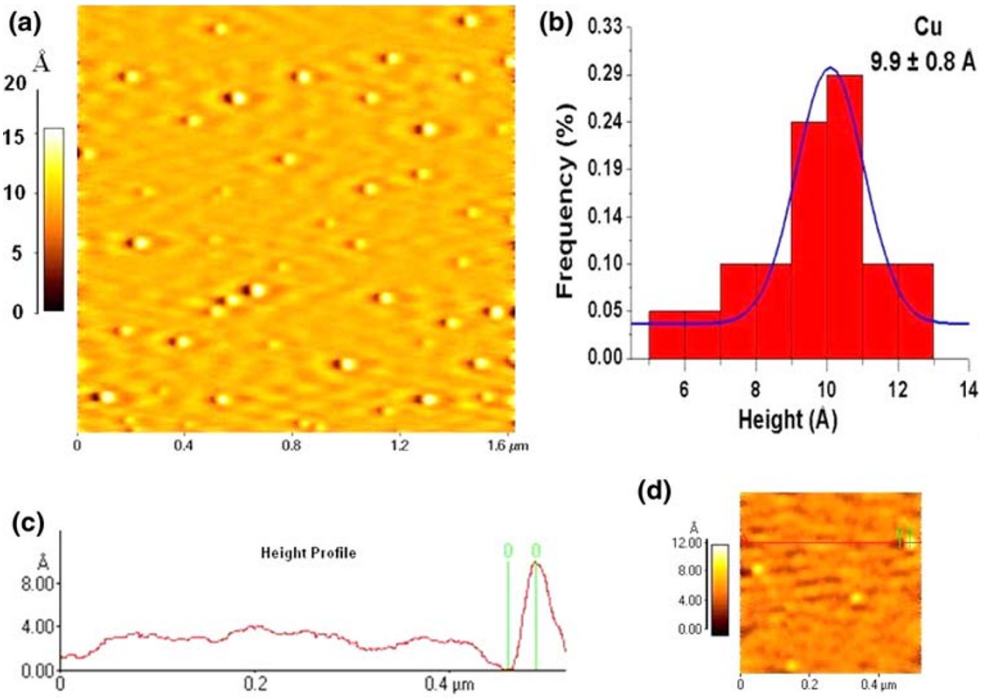

Fig. 7 **a** AFM topographical image from Cu nanoparticles deposited on sapphire and filtered in 1 nm, **b** Particle size histogram obtained from the height of the NPs, **c** Z-Height profile along the line indicated in (**d**), **d** Larger magnification from (**a**). Experimental conditions: Ar (10 sccm), He (25 sccm), Agg. Length (30 mm), Power (62 W)

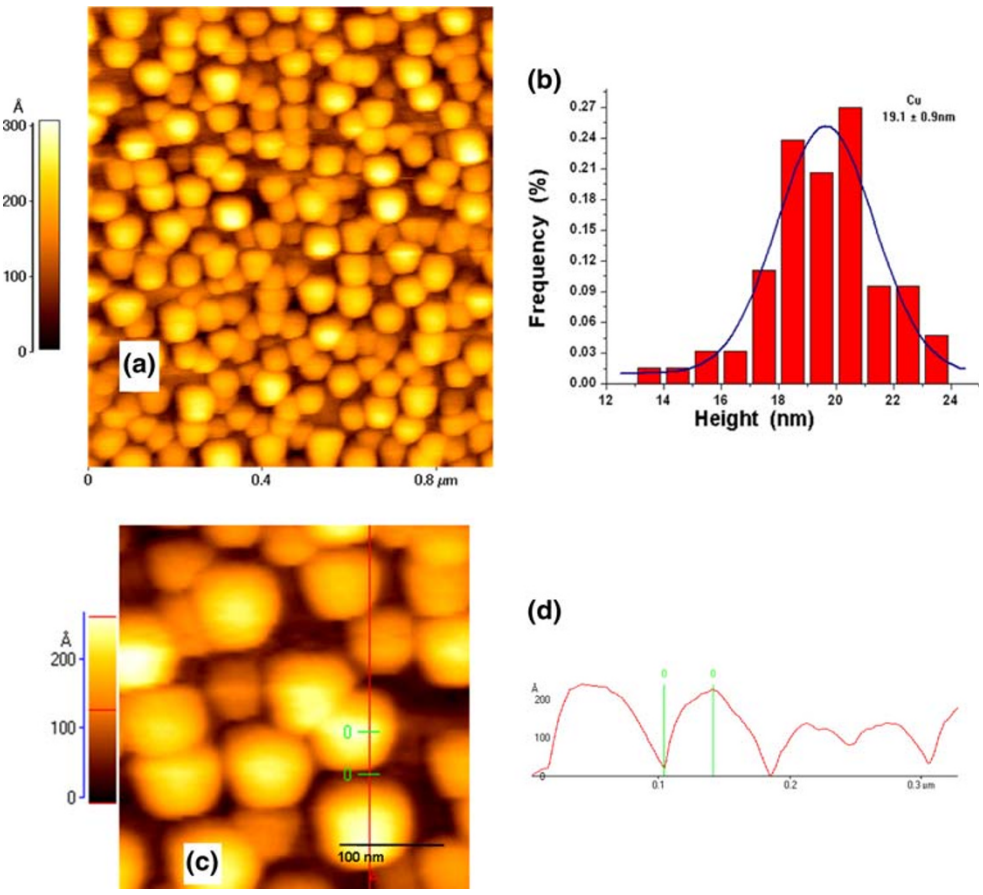

Fig. 8 **a** AFM topographical image from a Cu nanosized thin film deposited on Si and filtered in 20 nm, **b** Particle size histogram obtained from the height of the NPs, **c** Larger magnification of the film from (**a**), **d** Z-Height profile along the line indicated in (**c**), height (19.1 nm). Experimental conditions: Ar (25 sccm), He (2.2 sccm), Agg. Length (100 mm), Power (60 W)

deposited for one hour and filtered at 20 nm with the experimental conditions as indicated in Fig. 8. From this, we can observe that films are porous, since low-energy clusters tend to pile up on the substrate, leaving large cavities, which are desirable for retaining their high surface/volume ratio. From AFM observations, in Fig. 8a, we

note that the shape of nanoparticles is perfectly spherical and sized as they were filtered. Since the kinetic energy is negligible, compared to the bonding energy of an atom in the cluster, no fragmentation of the cluster occurs upon impact on the substrate. In this case, the height measurement (z-axis) shown in Fig. 8b was 19.1 nm and as previously, it was considered as its real size obtained through the height profiles, as shown in Fig. 8c and d. Statistical analysis made through these measurements is summarized in the histogram in (b). The Gaussian curve that fit to the data is centered in 19.1 ± 0.9 nm; this value is slightly deviated from the size predetermined experimentally but still maintains the low dispersion in size as in the case of monodispersed nanoparticles. The strict control of experimental parameters by IGC technique leads to obtain size-selected Cu clusters films, as a random stacking of nanometer-size crystallites assembly. Besides the importance of control size as Cu cluster films, it is important to understand how the size of these crystallites is determined and how stable the nanostructured film is. We can anticipate that the physical mechanism for cluster size evolution is, as in the monodispersed case, sintering by atomic diffusion. For thick films, however, surface diffusion can only be effective before a given cluster has been "buried" by the subsequent deposited Cu clusters. Thus, most of the size evolution takes place during growth, for later the physical routes to coalescence are expected to be much slower. For Cu thick films, a reasonable assumption is that a cluster impinging on a surface already covered by a layer of clusters does not diffuse, because it forms strong bonds with the layer of deposited Cu clusters. The process differs from submonolayer growth in two main ways: first, an impinging cluster has more than one neighbor; second, clusters are not free to move. These conditions make the Cu cluster film stable to the growing; hence, the size of the crystallites is comparable to the size of the free clusters. Low kinetics energy and contact angle are also crucial to determine the spherical geometry formed on the substrate. Clearly, further experimental and theoretical work is needed in order to confirm or invalidate our suggestions. Our actual research is linked to a clear understanding of the underlying mechanisms.

Summary

We have investigated the growth of Cu nanoparticles in a plasma enhanced sputtering gas aggregation type growth region. Various sputtering parameters were varied to observe the change in the size distributions of the nanoparticles. It was found that Ar flow rate favors the cluster growth but when this flow reach some critical value the mean cluster size decreases since Ar also sweep the cluster through the aggregation zone this reducing the time for particle growth. A continuous decreasing in mean cluster size was also observed with the increasing in He flow, which reveals its effective role to reduce the size by reducing the associated residence time in the aggregation zone. Cu nanoparticle size is also controlled with the sputtering power, a nearly linear relationship was found, however, the most determinant experimental parameter to control size seems to be the aggregation length. From STEM and AFM measurements, we found that nanoparticles were monodispersed with the selected size, this demonstrates the efficiency of IGC technique to obtain cluster with the desired size. Additionally, controlling experimental parameters by IGC technique leads to obtain size-selected Cu cluster films. The deposition of size-selected Cu clusters represents a novel method of preparing Cu nanostructures, with high potential in optical and catalytic applications.

Acknowledgments M. A. Gracia-Pinilla thank to PROMEP for their support through grant PROMEP/103.5/09/3905. The authors thank J. Sainz, J. Flores, and J. Aguilar for their technical help.

References

1. V.F. Puntes, K.M. Krishnan, A.P. Alivisatos, Science **291**, 2115 (2001)
2. F.S. Diana, S.H. Lee, P.M. Petroff, E.J. Kramer, Nano Lett. **3**, 891 (2003)
3. L. Qi, J. Ma, J. Shen, J Colloid Interf. Sci. **186**(2), 498 (1997)
4. P. Chen, X. Wu, J. Lin, K.L. Tan, J. Phys. Chem. B **103**(22), 4559 (1999)
5. N. Arul Dhas, C. Paul Raj, A. Gedanken, Chem. Mater. **10**(5), 1446 (1998)
6. H.T. Zhu, C.Y. Zhang, Y.S. Yin, J Cryst. Growth **270**, 722 (2004)
7. H. Ohde, F. Hunt, C.M. Wai, Chem.Mater. **13**(11), 4130 (2001)
8. S.S. Joshi, S.F. Patil, V. Iyer, S. Mahumuni, Nanostruct. Mater. **10**(7), 1135 (1998)
9. I.M. Goldby, B. Von Issendorff, L. Kuipers, R.E. Palmer, Rev. Sci. Instrum. **68**, 3327 (1997)
10. S. Yamamuro, K. Sumiyama, K. Suzuki, J. Appl. Phys. **85**, 483 (1999)
11. T. Hihara, K. Sumiyama, J. Appl. Phys. **84**, 5270 (1998)
12. E. Pérez-Tijerina, M. Gracia Pinilla, S. Mejía-Rosales, U. Ortiz-Méndez, A. Torres, M. José-Yacamán, Faraday Discuss **138**, 353 (2008)
13. M.L. Wu, D.H. Chen, T.C. Huang, Chem. Mater **13**, 599 (2001)
14. N.R. Jana, Z.L. Wang, T.K. Sau, T. Pal, Curr. Sci. **19**, 1367 (2002)
15. F. Kim, J.H. Song, P. Yang, J. Am. Chem. Soc. **124**, 14316 (2002)
16. N.R. Jana, L. Gearheart, C.J. Murphy, Chem. Commun. **7**, 617 (2001)
17. X. Liu, W. Cai, H. Bi, J. Mater. Res. **17**, 1125 (2002)
18. C. Huang, C.Z. Yang, Appl. Phys. Lett. **74**, 1692 (1999)
19. K. Akamatsu, S. Deki, J. Mater. Chem. **7**, 1773 (1997)
20. M. Kogiso, K. Yoshida, K. Yase, T. Shimizu, Chem. Commun. 2492 (2002)
21. J.A. Eastman, S.U.S. Choi, S. Li, W. Yu, L. Thompson, J. Appl. Phys. Lett. **78**, 718 (2001)
22. M. Zhao, L. Sun, R. Crooks, J. Am. Chem. Soc. **120**, 4877 (1998)

23. J.Y. Bigot, Phys. Rev. Lett. **75**, 4702 (1995)
24. T.S. Ahmadi, J. Phys. Chem. **100**, 8053 (1996)
25. M. Perner, Phys. Rev. Lett. **78**, 2192 (1997)
26. J.H. Kim, T.A. Germer, G.W. Mulholland, S.H. Ehrman, Adv. Mater. **14**, 518 (2002)
27. H.C. Choi, Y.M. Jung, S.B. Kim, Intl. J. Nanosci. **1**, 443 (2002)
28. Mantis Deposition Ltd. Oxford, England. www.mantisdeposition.com
29. J. Schiotz, T. Rasmussen, K.W. Jacobsen, O.H. Nielsen, Philos. Mag. Lett. **74**, 339 (1996)
30. M.Á. Gracia-Pinilla, D. Ferrer, S.J. Mejía-Rosales, E. Pérez-Tijerina, Nanoscale Res. Lett. **4**, 896 (2009)
31. Z.Y. Li, N.P. Young, M. Di Vece, R.E. Palmer, A.L. Bleloch, B.C. Curley, N.P. Young, R.L. Johnston, J. Jiang, J. Yuan, Nature **451**, 46 (2008)
32. B.C. Curley, R.L. Johnston, N.P. Young, Z.Y. Li, M. Di Vece, R.E. Palmer, A.L. Bleloch, J. Phys. Chem. C **111**, 17846 (2007)
33. R. Wang, O. Dmitrieva, M. Farle, G. Dumpich, M. Acet, S. Mejia-Rosales, E. Perez-Tijerina, M.J. Yacaman, C. Kisielowski, J. Phys. Chem. C **113**, 4395 (2009)